Journal of Volcanology and Geothermal Research 321 (2016) 18–30

Contents lists available at ScienceDirect

Journal of Volcanology and Geothermal Research

journal homepage: www.elsevier.com/locate/jvolgeores

Predicting eruptions from precursory activity using remote sensing data hybridization

K.A. Reath [a,*], M.S. Ramsey [a], J. Dehn [b], P.W. Webley [b]

[a] Department of Geology and Planetary Science, University of Pittsburgh, 4107 O'Hara Street, Pittsburgh, PA 15260, United States
[b] Geophysical Institute, University of Alaska Fairbanks, 903 Koyukuk Drive, Fairbanks, AK 99775, United States

ARTICLE INFO

Article history:
Received 2 October 2015
Received in revised form 21 April 2016
Accepted 27 April 2016
Available online 28 April 2016

Keywords:
Volcanology
Thermal
ASTER
AVHRR
Precursory
Kliuchevskoi

ABSTRACT

Many volcanoes produce some level of precursory activity prior to an eruption. This activity may or may not be detected depending on the available monitoring technology. In certain cases, precursors such as thermal output can be interpreted to make forecasts about the time and magnitude of the impending eruption. Kamchatka (Russia) provides an ideal natural laboratory to study a wide variety of eruption styles and precursory activity prior to an eruption. At Bezymianny volcano for example, a clear increase in thermal activity commonly occurs before an eruption, which has allowed predictions to be made months ahead of time. Conversely, the eruption of Tolbachik volcano in 2012 produced no discernable thermal precursors before the large scale effusive eruption. However, most volcanoes fall between the extremes of consistently behaved and completely undetectable, which is the case with neighboring Kliuchevskoi volcano. This study tests the effectiveness of using thermal infrared (TIR) remote sensing to track volcanic thermal precursors using data from both the Advanced Spaceborne Thermal Emission and Reflection Radiometer (ASTER) and Advanced Very High Resolution Radiometer (AVHRR) sensors. It focuses on three large eruptions that produced different levels and durations of effusive and explosive behavior at Kliuchevskoi. Before each of these eruptions, TIR spaceborne sensors detected thermal anomalies (i.e., pixels with brightness temperatures >2 °C above the background temperature). High-temporal, low-spatial resolution (i.e., ~hours and 1 km) AVHRR data are ideal for detecting large thermal events occurring over shorter time scales, such as the hot material ejected following strombolian eruptions. In contrast, high-spatial, low-temporal resolution (i.e., days to weeks and 90 m) ASTER data enables the detection of much lower thermal activity; however, activity with a shorter duration will commonly be missed. ASTER and AVHRR data are combined to track low-level anomalies months prior to an eruption and higher-energy events prior to large eruptions to develop a monitoring approach for this eruption style. Results show that strombolian eruptions produce enough energy in the pre-eruptive phase to trigger an AVHRR detection. Paired with ASTER data, the results can be extended back in time to develop a precursory timeline, which captures subtle changes in volcanic activity that would commonly go unnoticed in a single data set. Although these precursors may be volcano and eruption specific, the now sixteen-year-old database from ASTER allows this methodology to be repeatable at other volcanoes to establish a quantitative precursory baseline, which would be an improvement over current eruption classifications.

1. Introduction

With 29 currently active volcanoes, the Kamchatka Peninsula is one of the most volcanically active regions on Earth. Volcanic hazards such as lahars, pyroclastic flows, earthquakes, and ash-clouds have been associated with eruptions in this area. This moderate/high level of volcanic activity has long been an area of interest (e.g., Gorshkov, 1959; Fedotov, 1984; Fedotov and Masuerenkov, 1991; Casadevall, 1993; Belousov et al., 1999; Ramsey and Dehn, 2004; Carter and Ramsey, 2009). This subduction zone also contains a slab window between the Pacific, Komandrsky, and Okhotsk plates, occurring at the point where the Aleutian island arc meets Kamchatka, which leads to this increased volcanic activity and can alter magma compositions over relatively short distances (e.g., Yogodzinski et al., 2001; Portnyagin et al., 2005; Jiang et al., 2009; Koloskov et al., 2014). Carbon dating and detailed mapping of historic flows determined the activity at each volcano for the past 10 Ka–50 Ka (Braitseva et al., 1995), which identifies the most historically active volcanoes as: Kliuchevskoi, Bezymianny, Tolbachik, Kizimen, Sheviluch, Alny, and Gamhen volcanoes (Fig. 1). Many of these same volcanoes remain some of the most active in the region today. The hazards associated with these eruptions create a limited local risk due to the low population concentration (Rose and Ramsey,

* Corresponding author at: Department of Geology and Planetary Science, University of Pittsburgh, 4107 O'Hara Street, Pittsburgh, PA 15260, United States.
E-mail address: kar121@pitt.edu (K.A. Reath).

http://dx.doi.org/10.1016/j.jvolgeores.2016.04.027
0377-0273/

Fig. 1. Location map of the volcanoes found in the Kamchatka Peninsula with Kliuchevskoi volcano denoted in bold font. Modified from Rose and Ramsey, (2009).

2009). Larger scale eruptions, however, produce ash-clouds that pose an increased risk to the approximately 200 aircraft and 200,000 people that fly over the area daily (Miller and Casadevall, 2000). Recent volcanism in the region has been monitored with spaceborne data by the Kamchatka Volcano Emergency Response Team (KVERT) and the Alaskan Volcano Observatory (AVO).

Precursory activities of the volcanoes in this region (Fig. 1) are varied. For example, Bezymianny volcano tends to be somewhat predictable, with thermal energy released from the summit that gradually increases until an eruption occurs (Carter et al., 2008; Sobolevskaya and Senyukov, 2008; van Manen et al., 2010; van Manen et al., 2013). Conversely, Tolbachik volcano has a history of large scale fissure eruptions occurring with little to no interpretable thermal precursory activity (Edwards et al., 2013; Kugaenko et al., 2014). Kliuchevskoi volcano consistently produces precursory activity, however this activity has had limited application to predicting the size and duration of an upcoming larger eruption. With the current methods available to monitor thermal activity, only precursors days to weeks prior have been linked to an upcoming eruption at Kliuchevskoi. This type of activity is common to many volcanoes throughout the world (e.g., Francis and Rothery, 1987; Oppenheimer et al., 1993, Harris et al., 1997a; Dehn et al., 2002; Pergola et al., 2004; Pergola et al., 2009; Marchese et al., 2014). A more detailed study of the precursory history of Kliuchevskoi using the current suite of spaceborne TIR sensors could provide a methodological approach for volcanoes world-wide.

1.1. Monitoring of North Pacific volcanoes

During the 1989–1990 eruption of Redoubt volcano in Alaska, AVO developed a color-coded alert system for monitoring volcanoes and the associated risks (Guffanti and Miller, 2013). This system more effectively communicated volcanic activity levels to non-scientists. It has been modified in subsequent years and adopted by the International Civil Aviation Organization (ICAO) as the recommended alert-system for all volcano observatories world-wide. Although still somewhat qualitative, the AVO system is the only standardized international volcano alert protocol currently in use (Fearnley et al., 2012). The color codes used in this system (Green, Yellow, Orange and Red) represent lower to higher levels of concern and shorter time frames for the expected onset of eruption. The United States Geology Survey (USGS) now employs a similar system where the terms Normal, Advisory, Watch, and Warning replace Green, Yellow, Orange, and Red.

In Kamchatka, KVERT provides status reports of volcanic activity to the local authorities and international community regarding any imminent volcanic risk (Heiken et al., 1992; Schneider et al., 2000; Neal et al., 2009). These status updates are determined using an array of monitoring instruments, including seismic and GPS stations, ground-based visual and web camera observations, and low-spatial, high-temporal resolution orbital satellite data. The satellite data are collected and maintained by several groups such as the Moderate Resolution Imaging Spectroradiometer (MODIS) volcano archive (MODVOLC) used by KVERT (Dehn et al., 2000; Schneider et al., 2000; Wright et al., 2004). In addition, AVO and the University of Alaska Fairbanks (UAF) monitor data from the Geostationary Operational Environmental Satellites (GOES) sensor, which collects thermal infrared (TIR) data with an average pixel size of 4 km acquired every 15 min, the MODIS sensor with a 1 km TIR pixel size acquired every 4 to 6 h, and the AVHRR sensor, with 1 km TIR pixel size acquired every 15 min to 6 h.

Due to the large pixel size of these sensors, smaller and weaker thermal anomalies are not detected by these sensors. Therefore, subtle

changes in thermal flux, such as what is commonly produced in the initial stages of precursory activity, or spatially small thermal features, such as the appearance of new fumaroles at the summit, commonly go undetected. In some cases, however, seemingly random and isolated peaks in thermal activity are detected months to weeks before the onset of an eruption. These peaks in thermal output have been observed at Kliuchevskoi. Dehn et al., (2000) proposed that these are likely the result of strombolian activity, suggesting that a large sudden increase in thermal energy is produced from fresh material expelled during a strombolian eruption. The material then rapidly cools, resulting in a rapid decrease in thermal output. Therefore, examining changes in thermal activity with a sensor unable to detect lower levels of thermal output results in these singular and seemingly isolated spikes being the only indication of an eruption. In order to capture the entire thermal flux record related to the many styles of subtle thermal precursory activity, a sensor with a higher-spatial resolution and better radiometric accuracy is required.

1.2. ASTER

The ASTER sensor is one of the five instruments on the National Aeronautics and Space Administration (NASA) Terra satellite, which was launched in December 1999. ASTER has 15 m per pixel spatial resolution with three wavelength channels in the visible/near infrared (VNIR) and 90 m per pixel spatial resolution with five wavelength channels in the TIR. With this high spatial resolution and a 60 km swath width, the temporal resolution is limited to 1–5 days at higher latitudes and 16 days at the equator (Yamaguchi et al., 1998; Ramsey and Dehn, 2004). The ASTER TIR sensor has a modeled noise equivalent delta temperature (NEΔT) of between 0.15–0.3 °C, allowing accurate temperatures to be derived following atmospheric correction and temperature/emissivity separation. (Gillespie et al., 1998). Another unique aspect of ASTER is that it is scheduled daily, which affects the amount of coverage acquired and later processed. This schedule is created by individual user requests, global mapping campaigns, and emergency requests for acquisitions (Yamaguchi et al., 1998). In late 2006 the ASTER Urgent Request Protocol (URP) was implemented, which allows an automatic request for ASTER data to be triggered by the detection of thermal anomalies from an array of low spatial resolution sensors (Ramsey, 2015). For example, whenever the AVHRR senor detects a volcano related thermal anomaly via the AVO monitoring program currently in place, the URP system is triggered and an ASTER observation is scheduled for the next available overpass (Ramsey and Dehn, 2004; Duda et al., 2009; Ramsey et al., 2004). Whereas this system does not provide real-time data, it does expedite the ASTER scheduling/acquisition/processing pathway, providing data to users as quickly as possible (Carter et al., 2008; Ramsey, 2015). This increase in temporal resolution of ASTER data has improved the sensors efficiency to capture thermal flux data over the given time span. That, combined with the moderately high spatial and accurate radiometric resolution of the ASTER TIR array, makes the data more sensitive to thermal flux from these smaller anomalies, thus improving the detection of thermal precursory activity prior to an eruption.

1.3. Data hybridization

The ASTER, AVHRR and MODIS instruments have strengths and weaknesses that impact the analysis of thermal infrared data for precursory activity. The high spatial resolution of ASTER allows detection of subtle changes in low-grade thermal energy output and also produces a more detailed thermal image of the surface (Fig. 2A). The high temporal resolution of both the AVHRR and MODIS instruments greatly improve the ability to capture events occurring on shorter time scales. Both MODIS and AVHRR data are less useful for differentiating background temperatures unaffected by volcanogenic activity from those associated with thermal anomalies (Fig. 2B and 2C). However, valuable

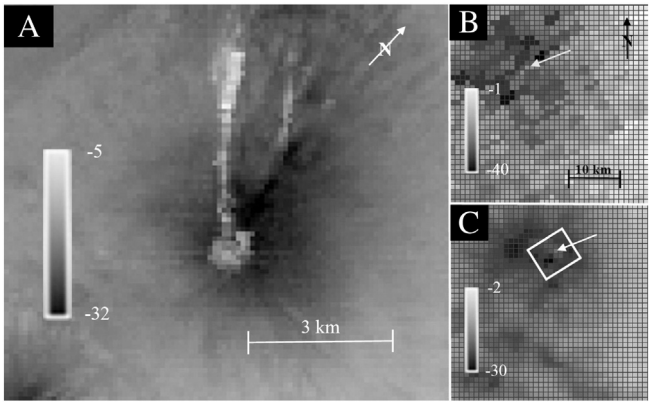

Fig. 2. Thermal infrared brightness temperature data of Kliuchevskoi volcano (temperatures in degrees C). (A) ASTER data acquired on April 25, 2009 at 10:51 UTC. (B) MODIS band 21 (3.96 μm) data acquired on April 26, 2009 at 09:53 UTC. (C) AVHRR band 3 (3.74 μm) data acquired on April 26, 2009 at 09:13 UTC. The images in Both B and C are retrieved from the Okmok algorithm used to monitor volcanoes in the North Pacific and are tiled to better differentiate pixels. The white arrows in images B and C denote the location of Kliuchevskoi, with the white box in C showing the area in A.

information can be extracted from the combined datasets of all these instruments. The presence of detectable thermal anomalies in the AVHRR and MODIS data are the result of brief large outputs of thermal energy, which have been interpreted to be associated with strombolian eruptions. Where compared to ASTER data, these strombolian events commonly coincide with variations in the trend of thermal flux at the summit, this correlation plays an important role in understanding precursory mechanisms.

1.4. Strombolian eruptions

Strombolian eruptions are commonly observed during periods of activity at Kliuchevskoi (Menyailov, 1975; Rose and Ramsey, 2009; van Manen and Dehn, 2009; Smithsonian Global Volcanism Program, 2013). Past research on these eruptions has shown that they likely originate from the bursting of a gas slug at the magma free surface (Macdonald, 1972; Chouet et al., 1974; Blackburn et al., 1976; Ripepe et al., 1993; Vergnioelle and Brandies, 1996; Patrick et al., 2007). Whereas the exact method of the formation of this gas slug is a point of debate each method shares several common points (Parfitt, 2004). First, the volcanic gases within the magma form bubbles that eventually coalesce into an expanding gas slug (Parfitt and Wilson, 1995; Vergnioelle and Brandeis, 1996). As the gas slug moves up the volcanic conduit, it continues to gain volume and expand from the continued addition of gas (Kirchdorfen, 1999; Chouet et al., 1999). Finally, once the gas slug reaches a shallow depth with a minor amount of over pressure (~0.5–4 bar, Ripepe and Marchetti, 2002) the slug bursts through the magma surface, resulting in an eruption of ballistics and increased output of gas (Blackburn et al., 1976). After the expulsion of the slug, the upward driving mechanism and the additional volume from the gas have been removed. Therefore, the height of the magma in the conduit will drop, which may lead to backfilling of the conduit from the slumping of inner crater walls (Calvari and Pinkerton, 2004) or from the rollback of explosion ejecta into the vent (Booth and Walker, 1973; Self et al., 1974; Francis, 1993). This backfill increases the overpressure and can lead to additional eruptions which, clear the vent produce ballistics and ash (Patrick et al., 2007).

1.5. Kliuchevskoi eruptions of interest

Of the 29 active volcanoes in Kamchatka, Kliuchevskoi is one of the most active, producing an average of 6.0×10^7 tons of material per year (Fedotov et al., 1987; Fedotov and Masurenkov, 1991; Ozerov et al., 1997). In the past 21 years flank, summit, and paroxysmal type

eruptions have all been recorded (Fedotov and Masurenkov, 1991; Rose and Ramsey, 2009). Sixteen flank eruptions have occurred since 1907 and the last paroxysmal summit eruption was in 1994. Eruptions from the summit crater are the dominant type, occurring every 1–2 years in the past century (Fedotov and Masurenkov, 1991; Smithsonian Global Volcanism Program, 2013). These eruptions vary from strombolian to plinian in scale and have a longer duration than flank eruptions (Gushchenko, 1979; Rose and Ramsey, 2009; Smithsonian Global Volcanism Program, 2013).

In 2005, 2007 and 2009 Kliuchevskoi produced eruptions large enough to be classified as a Volcanic Explosive Index (VEI) of 2, and in the case of both the 2005 and 2009 eruptions, a VEI 1 eruption was believed to have reached its conclusion 6–8 months before the VEI 2 eruption of interest (Smithsonian Global Volcanism Program, 2013). In 2007, a relatively long period of time of assumed inactivity passed before the onset of the eruption. Seemingly random and isolated thermal anomalies (e.g., Dehn et al., 2000) were seen in the AVHRR data before each of these eruptions. However, without higher spatial resolution data, these anomalies were not linked to the onset of a larger eruption. The onset of each eruption was not predicted for a period longer than days to a week before according to analysis of the AVO daily reports and Dehn and Harris, (2015). Although this does allow for a warning to be issued before large eruptions, mitigation of potential hazards beyond evacuation or avoidance becomes extremely difficult in this time scale. This study therefore seeks to improve this time by improving our understanding of the precursory period and the activity therein by incorporating ASTER data into the existing satellite-based monitoring dataset. A more complete understanding of the eruptive precursors should allow the warning time to an eruption onset to be greatly extended, thus lowering the associated risks.

2. Methods

2.1. Data collection

All data acquired by orbital instruments during the precursory time periods for the Kliuchevskoi eruptions were initially inspected using the US Geological Survey (USGS) Global visualizer viewer (Glovis) and University of Alaska Fairbanks (UAF) Volcanic Ash Detection, Avoidance, and Preparedness for Transportation (V-ADAPT, Inc.) program. All available cloud-free scenes over the summit were selected. In the case of the AVHRR and MODIS data, only images where a summit thermal anomaly could be distinguished from background were included.

2.2. Period of analysis

The thermal activity produced at the summit of Kliuchevskoi prior to the large eruptions in 2005, 2007, and 2009 was analyzed in detail. The data were constrained to a time period in which thermal activity can be directly related to the precursory activity of these eruptions. This time period in both the 2005 and 2009 events occurs between the inactivity preceding, the VEI class 1 eruption and the onset of the VEI class 2 eruption. This chosen time period precludes thermal anomalies related to prior eruptive phases from being classified as precursory activity. This time period extends from September 15, 2004 to January 20, 2005 and from April 16, 2009 to August 1, 2009 (Smithsonian Global Volcanism Program, 2013) respectively for the 2005 and 2009 events. The precursory period of the 2007 eruptive phase is different than the other two eruptions. In 2007, there was no VEI 1 eruption 4–6 months before the onset eruption on February 15, 2007. The prior eruptive cycle was classified as inactive on April 7, 2005 (Smithsonian Global Volcanism Program, 2013), resulting in an inactive period of approximately 21 months between eruptions. This presented a unique opportunity to greatly extend the period of precursory analysis, which was chosen to be one year to quantify the inactive phase of Kliuchevskoi as well as the onset of precursory activity. Within this one-year period, enough data were captured to positively define all 3 phases of precursory activity.

2.3. Data processing

ASTER radiance-at-sensor data were atmospherically corrected to surface radiance using the standard Level 2 (AST_09T) product (Thome et al., 1998; Abrams, 2000). Emissivity and brightness temperature were separated for each pixel using the emissivity normalization approach (Gillespie, 1985; Realmuto, 1990; Reath and Ramsey, 2013). This process relates radiance to emissivity and temperature using the plank equation and produces a unique emissivity image for each of the five ASTER TIR channels available and one brightness temperature image for the entire scene. AVHRR and MODIS infrared data were converted directly into radiant temperature in near real time using the Okmok algorithm and archived by UAF (Dean et al., 1998; Dehn et al., 2000; Bailey et al., 2010). Only AVHRR band 3 (3.74 μm) data (3B in AVHRR-15 and later) and MODIS band 21 (3.96 μm) data were included in this analysis. These bands correspond to the wavelength region most commonly used to detect high heat sources, such as volcanoes and fires (Dehn et al., 2000; Ramsey and Dehn, 2004; Pergola et al., 2004).

A background temperature is first calculated for each brightness temperature image. In the ASTER data the background temperature is calculated by averaging the temperatures from an 11 × 11 pixel (9.8×10^5 m^2) region of interest (ROI) within 1 km and at approximately the same elevation as the observed thermal anomaly. The area of the ROI was chosen specifically to approximate the size of an AVHRR and MODIS TIR pixel and capture any smaller-scale pixel to pixel temperature variations. These ROIs are geolocated at the same latitude and longitude in every ASTER scene and confirmed free of thermally-anomalous pixels and clouds. Background temperatures for AVHRR data are determined by calculating the temperature of a pixel adjacent to the thermally anomalous area with no perceived temperature artifacts, such as (1) pixel bleeding, from an adjacent high-temperature anomaly (Dehn et al., 2002; Harris et al., 1997b, 1999); (2) a thermal rebounding artifact ("recovery pixel") created by miscalculating the radiance value of the pixel directly adjacent to a thermally-elevated pixel; (3) cosmic ray hits; (4) station mask transmission errors; and/or (5) clouds. Using a single pixel for background temperatures is a commonly used approach where identifying volcano thermal anomaly temperatures using the Okmok algorithm (Dean et al., 1998; Dehn et al., 2000; Schnieder et al., 2000; Dean et al., 2002; Dehn et al., 2002; Webley et al., 2013). Due to the multitude of factors affecting the AVHRR data and the abundance of AVHRR scenes analyzed in this process, finding a single geo-located pixel to be used as the background value for every scene was not possible.

The specific criteria needed to classify a pixel as containing a thermal anomaly are discussed in detail by Pieri and Abrams (2005), who refer to thermal anomalies as pixels containing elevated thermal activity. This elevated activity increases the amount of radiant energy, which is directly related to an increase in brightness temperature from that pixel. This does not affect the background pixels, if chosen correctly. The radiometric accuracy for ASTER brightness temperatures using the emissivity normalization approach is ±1–2 °C (Thome et al., 1998) and ±2.5 °C for AVHRR, both assuming a natural environment with atmospheric integrated water vapor (Goita and Royer, 1997). Therefore, anything less than 2 °C above the derived background temperature would be indistinguishable from noise and not distinguished in this analysis. A value of 2 °C above the background temperature was therefore chosen as the threshold, above which a pixel is considered thermally anomalous. The distribution of anomaly temperatures in the ASTER data are determined by including only pixels over the summit area affected by increased thermal output in an ROI and using the pixel with the highest temperature in this area. The reason for using the pixel with the highest temperature rather than the average temperature of the region is twofold. First, the area affected by the thermal

anomaly does not remain constant. Analyzing the total area would introduce fluctuations in both total area and derived temperature to determine the total amount of heat produced. However, by only examining the hottest pixel, the area remains constant and only the most intense thermal output is tracked. Second, vent temperature fluctuations are more extreme than those of the entire thermal anomaly. In most cases, the vent is captured by one or two of the hottest pixels. This guarantees that only heat variations from the vent are used.

Thermal anomalies in the AVHRR ad MODIS data were typically dominated by one pixel, once again producing the highest temperature. This pixel can be related to the rapid thermal spikes recorded at the summit of Kliuchevskoi. MODIS and AVHRR capture data at a higher temporal resolution than ASTER and can therefore be used to increase the number of measured temperatures in the temporal dataset. The higher temporal resolution in the AVHRR and MODIS datasets also increases the probability of cloud-free scenes and capturing short-lived/high thermal output events, such as a strombolian eruption. However, in this study, confirmed thermal anomalies on the summit of Kliuchevskoi were only identified by MODIS within a week of the eruption onset. During this period of eruptive activity AVHRR data also produced abundant results and therefore the inclusion of MODIS data was deemed unnecessary.

The background temperatures derived in each of these scenes is subtracted from the thermal anomaly temperature in order to calculate the thermal anomaly temperature above background (ΔT_{ta}). The only factors that would change the derived background temperatures are environmental (e.g., time of day, season, local slopes, etc.) rather than volcanogenic. Therefore, the process of subtracting the background temperature also allows for the removal of these artifacts. These ΔT_{ta} data are plotted against time for the analysis period to determine the presence of any volcanic precursors. The plots are analyzed for patterns that lead to the better understanding of precursory processes, which in turn can indicate the possibility of an upcoming eruption. Although AVHRR data are connected in these plots, this is only to improve the graphic representation of the progression of points through time. Any period longer than six hours between AVHRR-derived temperatures is likely the result of no discernible thermal anomaly. In some cases, patterns that are related to events require further analysis. Where this occurred, combined analysis of the ASTER and AVHRR data spanning the event period proved useful to understand the processes responsible for these patterns.

In cases that required further analysis, the brightness temperature data are compared to the next available clear ASTER scene to examine the smaller-scale spatial variations occurring at the summit. These analyses are both qualitative (e.g., observing the locations of the hottest pixels) and quantitative (e.g., using the ROI approach to find the total area and average temperatures). It is likely that, in some cases, AVHRR recorded a thermal anomaly smaller than its pixel size. In order to produce an accurate reading of the average temperature of the thermal anomaly, the integrated pixel equation (Rothery et al., 1988) was applied to the AVHRR pixels affected by the thermal anomaly:

$$T_{pixel} = T_{hot}\left(\frac{A_{hot}}{A_{pixel}}\right) + T_{cold}\left(\frac{A_{pixel} - A_{hot}}{A_{pixel}}\right). \quad (1)$$

In this equation: T_{pixel} = original pixel(s) temperature, T_{hot} = temperature of hot feature, T_{cold} = temperature of cool feature, A_{hot} = area of hot feature, and A_{pixel} = total area cover by all pixel(s) included in equation. The equation is solved for T_{hot}, or the temperature of the hot feature within the pixel of interest. This approach is typically not required for the higher spatial resolution of the ASTER data as it is assumed that the hot fraction fills most/all of the ASTER TIR pixels. Therefore ASTER data can provide an area for the hot feature or A_{hot} and T_{cold}, or the background temperature is gained from the temperature of the background AVHRR pixel.

2.4. Analysis of the 3 eruptive cycles

Each eruptive cycle provides a unique insight into what is occurring during the precursory phase and how the data can be interpreted. It is important to note that when these two datasets are analyzed, two very different features are being represented. Due to the small area of the summit vent (several hundred meters maximum), flux related to changes in thermal output is only observed with a high spatial resolution sensor, such as ASTER. AVHRR and MODIS data cannot detect low-level thermal flux, instead recording short-lived/high temperature events. As mentioned, these measurements are not continuous. Each peak in AVHRR thermal output likely corresponds to a single strombolian event but only one temperature increase is recorded due to the rapid cooling following the eruption. In order to properly analyze these datasets, the data from each sensor must be considered independently and the differences between ASTER and AVHRR considered carefully.

The 2009 eruptive cycle contains the most complete dataset and is therefore analyzed first using the results as the control of a typical four month period before an eruption. In this dataset, peaks in the AVHRR-derived temperature data were further analyzed for strombolian activity. The added time period of the 2007 eruption was examined in order to extend the transition from inactivity to precursory activity. It was also used to determine what processes may have caused this eruption to escalate to a VEI 2 eruption without evidence of an initial VEI 1 phase seen in the other eruptions. The 2005 eruption data had the least amount of available data as the eruption occurred prior to the ASTER URP system being fully implemented. These data were examined to demonstrate how the URP system improved the understanding of volcanic processes and how volcanic precursors can be derived from even a limited amount of ASTER scenes.

3. Results

3.1. 2009 Eruptive cycle

Analysis of the precursory data from the 2009 eruptive cycle revealed several important features (Fig. 3). First, the spike in thermal output recorded in AVHRR data on May 21, 2009 19:32 UTC was analyzed to determine the possibility that it was the result of strombolian activity. The ASTER data acquired 11 days prior (May 10, 2009 00:32 UTC) and five days after (May 26, 2009 00:33 UTC) this event was analyzed. The difference in thermal activity is apparent on and around the summit (Fig. 4). In the center of Fig. 4A is the summit of Kliuchevskoi where a small cooling flow can be observed on the northwest (NW) flank produced during the previous VEI 1 eruption. No other thermal anomalies are observed. Later, a large thermally-elevated area on the southeast (SE) flank of the edifice is observed and the flow seen in the previous image is larger and more pronounced (Fig. 4B). The maximum pixel temperature on the SE flank has increased 33 °C from the previous image and is an average of 17 °C above the background temperature. Both of these scenes are captured within one minute of each other 16 days apart, thereby eliminating any possibility of environmentally-related thermal artifacts in the derived background temperature. The increase in both thermal output and areal extent of thermally-elevated pixels can only be the result of the deposition of volcanic material on the surface. The thermally integrated pixel Eq. (1) was used to determine whether the activity was intense enough to produce the observed temperature spike in the AVHRR data acquired on May 21, 2009 19:32 UTC. The result equates to an average deposition temperature of 46.4 °C above the background. The deposit also produced enough material to be detected as a thermal anomaly 17 °C above background in the ASTER scene (Fig. 4B). Additionally, a majority of the heat from this event had dissipated by the next clear AVHRR acquisition, approximately 1.5 days later on May 27, 2009 20:02 UTC where the average temperature of deposit had decreased to 5.9 °C above background

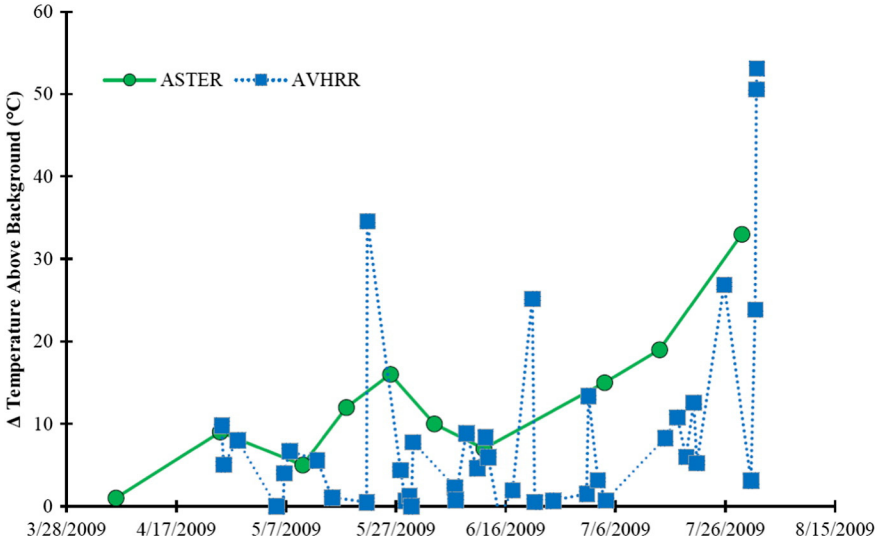

Fig. 3. Temperature versus time plot of the 2009 activity at Kliuchevskoi volcano (dates in US standard format, M/D/Y). The temperature difference represents the elevated crater temperature minus the background temperature. Data were gathered from April 25, 2009 until the onset of the eruption (August 1, 2009).

temperatures. These temperatures suggest relatively rapid cooling after the deposit was emplaced. This would result from a thin-mantling deposit similar to the spatter common following strombolian eruptions. It is important to note here that although these flows produce thermally anomalies, they are not located at the summit and therefore are not directly related to longer-term thermal output from the system.

With this understanding of the AVHRR temperature data, the ΔT_{ta} versus time can be examined further (Fig. 3). Over the entire study period, the ASTER data records the total thermal flux emanating from the summit, which results in an overall trend of an increase in temperature until the onset of the VEI 2 eruption. The AVHRR data are more sporadic with no observable trend until July 25, 2009, where the temperatures begin to steadily increase. However, analyzing these two datasets together reveals more information about the possible events leading up to the eruption. Importantly, fluctuations between short-term increases and decreases in ASTER-derived temperature coincide with increases in both intensity and the rate of thermal spikes in AVHRR data. Assuming these spikes are the result of strombolian eruptions, a link between the occurrence of these eruptions and the changes in thermal output can be observed (Fig. 3). From June 12, 2009 until the onset of the eruption on July 31, 2009 a consistent and rapid increase in thermal output is observed in the ASTER data, regardless of the trend in the AVHRR data. This increase in thermal output reaches levels high enough to be finally be detected in both AVHRR and ASTER data on July 25, 2009. At this point the precursory activity was detected by the AVO monitoring system. Six days before the eruption, AVO staffs were able to confirm that activity at Kliuchevskoi had increased. However, the activity level was not raised from green to yellow on August 1, 2009 after a tephra plume was detected.

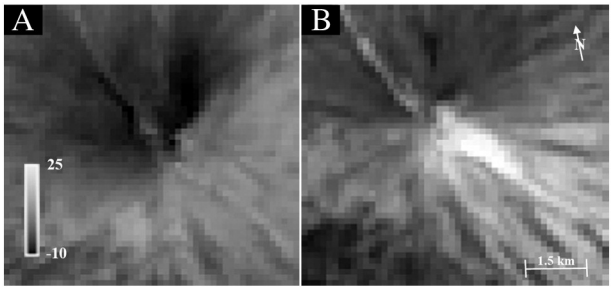

Fig. 4. ASTER thermal IR brightness temperature data of Kliuchevskoi Volcano collected on May 10, 2009 at 00:32 UTC (A) and May 26, 2009 at 00:33 UTC (B). A strombolian eruption likely occurred on May 21, 2009 and a region of elevated temperatures on the southeast flank can be seen, formed by the still-cooling erupted material. The temperature range is constant in both images (°C above background).

3.2. 2007 Eruptive cycle

The 2007 precursory data (Fig. 5) produced similar results to the 2009 analysis, with several important distinctions. First, there is a larger time period between eruptions before this eruptive phase, which allows the precursory data to be analyzed over a truly inactive period. During this phase the heat from the vents of the summit maintained a consistent temperature of approximately 10 °C above background for a period of eight months, lasting from January 3, 2006 to August 7, 2006 (Fig. 5). This inactive period is hereby referred to as Phase I. The end of Phase I is marked by a repeat of the variable thermal output observed in the 2009 precursor data. This variable thermal output phase (Phase II) lasts for approximately 4 months, from August 7, 2006 until December 22, 2006. The final phase (Phase III) last for approximately two months, from December 22, 2006 to February 15, 2007, and is once again characterized by an increase in thermal output at a relatively consistent rate leading up to the onset of eruption. However, in this case, Phase III does not increase as consistently as found in the 2009 data. From January 16–29, 2007 there is a 2-week period where the thermal output is diminished in both ASTER and AVHRR data. With this exception, the precursory activity of Phase II and III behaves nearly identically to behavior seen prior to the 2009 eruption. However, in this eruptive cycle Phase II lasts 2 months longer than in 2009, which is likely the result of precursory activity being recorded and analyzed over a longer time period. Phase II transitioned to Phase III 56 days before the onset of eruption in 2007, this same period lasted 49 days in 2009.

Phase III contains one large fluctuation in thermal output (Fig. 5). In order to further analyze the cause of this rapid drop in thermal activity, the ASTER TIR scenes acquired directly before the event on January 14, 2007, during the event on January 21, 2007, and directly after the decrease in heat on February 15, 2007 were analyzed in more detail (Fig. 6). Observation reveals that the data captured before the thermal decrease (Fig. 6A) show a large amount of heat being produced in four centrally located pixels with a maximum temperature of 38 °C and an average temperature of 5 °C above the background. The total area of the thermal anomaly at the crater is 0.75 km^2. In the second time frame (Fig. 6B) the thermal anomaly expanded to 0.79 km^2, and the average temperature decreased to 4 °C above background. In the third time frame (Fig. 6C) the maximum temperature again increases to

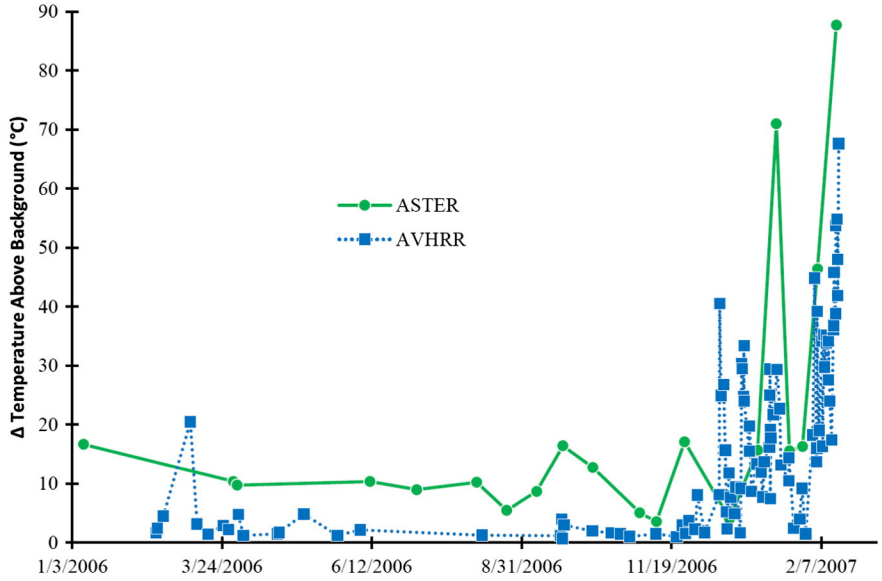

Fig. 5. Temperature versus time plot of the 2007 activity at Kliuchevskoi volcano (dates in US standard format, M/D/Y). Data were gathered for a period one year before the VEI classification 2 eruption that occurred February 15, 2007.

41 °C, measured from several pixels in the same location as those observed in the January 14, 2007 scene (Fig. 6A). The thermal anomaly in Fig. 6C has also decreased in area to 0.67 km^2 whereas the average temperature has risen to 6 °C above background. Immediately after this large decrease in thermal output, temperatures at the summit begin to increase rapidly and within ten days a VEI 2 eruption begins.

3.3. 2005 Eruptive cycle

The precursory activity before both the 2009 and 2005 eruptions are generally similar. In both cases a VEI 1 eruption occurred at least 5 months prior to the subsequent VEI 2 eruption. AVHRR thermal spikes appear to occur at similar intervals with slightly different intensities. The significant data difference between the 2005 and 2009 eruptive cycles is the number of ASTER scenes available (Fig. 7). Increased ASTER data frequency occurred directly after the implementation of the ASTER URP program, which went into place in late 2005 (Duda et al., 2009; Carter and Ramsey, 2010; Ramsey, 2015). The benefits of this program are evident and provide insights into the benefits of future higher spatial/higher temporal resolution instruments. Whereas the number of clear scenes recorded during 2009 allowed for a clear interpretation of the activity leading to the eruption, only three clear scenes were acquired during in the precursory period in 2005 (Fig. 7). It is therefore difficult to extract any meaningful trends with so few data points. However, visually examining the three ASTER scenes does provide some valuable clues (Fig. 8). In the first scene (Fig. 8A) a single pixel within the summit thermal anomaly produced an elevated thermal output compared to the surrounding pixels. In the second scene (Fig. 8B) this pixel no longer has an elevated temperature and all pixels within the anomaly have a relatively uniform temperature. The third scene (Fig. 8C) was acquired less than a week before the onset of the larger eruption. In this scene, a single pixel of elevated temperature relative

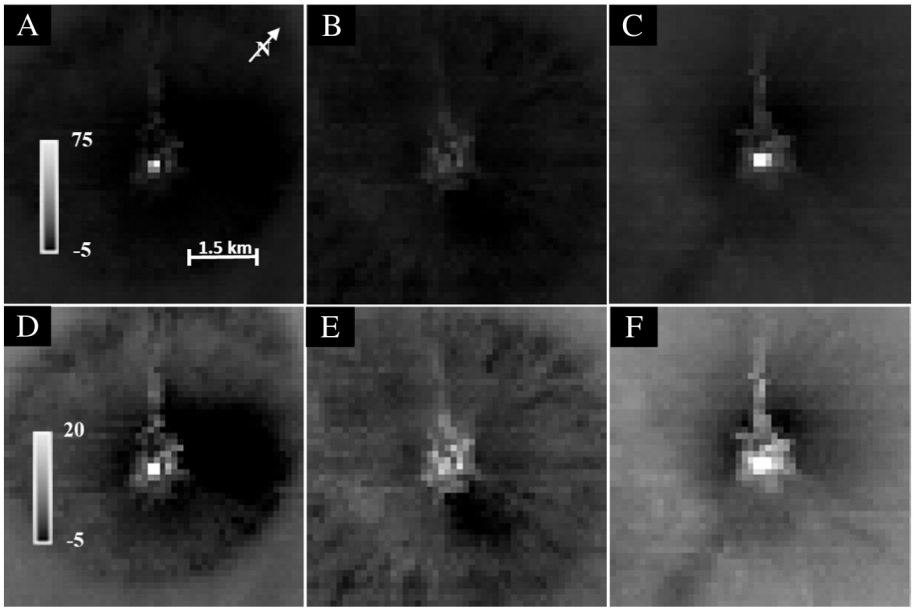

Fig. 6. ASTER images centered on Kliuchevskoi volcano captured (A, D) January 14, 2007 at 10:50 UTC, (B, E) January 21, 2007 at 10:56 UTC, and (C, F) February 15, 2007 at 10:50 UTC. Two different temperature ranges, (A–C) −5 to 75 °C and (D–F) −5 to 20 °C above background temperatures are shown to better highlight all surface features.

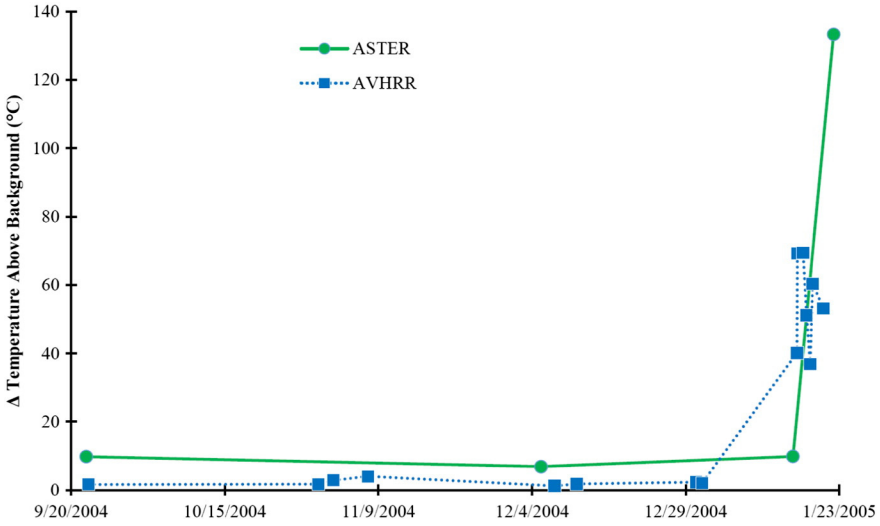

Fig. 7. Temperature versus time plot of the 2005 at Kliuchevskoi volcano (dates in US standard format, M/D/Y). Data were gathered for the period between September 15, 2004 VEI classification 1 eruption and the February 20, 2005 VEI classification 2 eruption.

to background can once again be seen in the crater. The location of that pixel has changed, however. Whereas these data to do not provide the same level of quantifiable data as the 2007 and 2009 data series, thermal variability can still be observed at the summit.

4. Discussion

4.1. Precursory phases

Fluctuations in the thermal output over time (Phase II) prior to the onset of eruption were observed in each of the case studies. Whereas the lack of ASTER data before the 2005 eruption prevented these fluctuations from being as clearly tracked as the 2007 and 2009 eruptions, examination of the individual ASTER scenes suggest that these fluctuations were still occurring. Furthermore, a pattern can be distinguished in the precursory activity of all three eruptions. During the restive phase (Phase I) there is a consistent, low-level thermal output from the summit crater only detectable with ASTER data. These periods last from months to years. The ASTER data gathered during the 2007 precursory period showed that thermal variations were present approximately 6 months prior to the eruption (Phase II).

Following this phase, the thermal output from the summit begins to increase as gas begins to build in the conduit and a gas slug is formed. The gas slug expands with time and rises, driving the magma higher in the conduit. This results in an increase in thermal output and a larger thermal anomaly at the summit. After the strombolian eruption, this gas slug becomes depleted. As a result the height of the magma in the conduit and the thermal output both decrease. This cycle appears to repeat periodically throughout Phase II in some cases. In others, when this drop in magma height occurs, backfilling of the conduit from slumping of the inner crater walls or the rollback of explosive ejecta, produces a transition from a decreasing thermal output to an increasing one. This backfill is cleared from the conduit once the gas slug has been reestablished in the conduit. Patrick et al. (2007) describes that these eruptions should be accompanied by a small ash cloud, which may be occurring and visible at the site. However, such a cloud was not large enough to be detected by either ASTER or AVHRR. Once this backfill has been cleared, the gas slug and magma levels once again rise in the conduit and the cycle repeats (twice in 2009 and 2.5 times in the 2007).

After several sequences of Phase II activity, the volcanic activity transitions to Phase III. Here, thermal output consistently increases until the onset of eruption. The ASTER data suggests that Phase III begins approximately 2.5 months prior to the onset of the large, ash-producing VEI 2 eruption in 2009 and approximately 2 months before the onset in 2007. In the 2007 data, increased temporal resolution and numerous clear scenes at the time of this transition from Phase II to Phase III allowed the ASTER and AVHRR data to be directly compared. During this transition in ASTER data, a large strombolian eruption was recorded in the AVHRR data. This eruption most likely cleared and/or expanded the conduit allowing for a decrease in the confining (or lithostatic/overburden) pressure on the magma chamber, causing the ascent of magma toward the surface. As the magma rose in the conduit, thermal output increased and the driving mechanism controlling magma height shifts from the gas slug to consistently rising magma in the conduit. In prior studies, similar Phase III behavior has been noted by Pieri and Abrams (2005) in their observations of the precursory activity at Chikurachki volcano in 2003 using ASTER data.

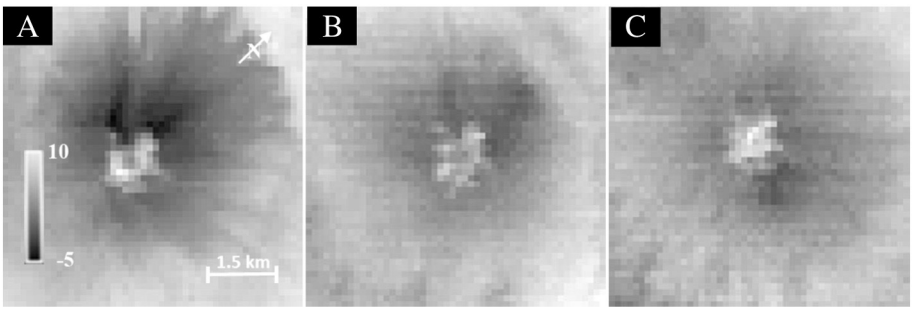

Fig. 8. ASTER image data centered on Kliuchevskoi volcano captured (A) September 2, 2004 at 10:49 UTC, (B) December 5, 2004 at 11:01 UTC, and (C) January 15, 2005 at 10:55 UTC. The temperature range is constant in all images (degrees C above background).

These three phases produce distinctly different thermal variability over time due directly to the differing precursory activity. Examining the ASTER time series for a particular phase allows the current hazard state to be assessed and the approximate time before a larger eruption to be determined. Evaluating the transition from a constant thermal output (Phase I) and a variable thermal output (Phase II) can be accomplished easily given a large enough dataset. Once the ASTER-derived temperature at the crater varies more than 2 °C per week, activity transitions to Phase II. However, the transition between Phase II and Phase III is more subtle. In the 2007 data, a large thermal spike in the AVHRR data was observed at the same time the ASTER data transitioned to a consistent increase in thermal output. This spike is greater than any previously recorded in the cycle, suggesting a larger strombolian eruption. This eruption likely cleared and expanded the volcanic conduit reducing the confining pressure on the magma chamber, allowing magma to ascend and resulting in a consistent increase in thermal output. Because this larger strombolian eruption initiates this magma driven ascent, the indicator that signifies the transition to Phase III is the large spike in thermal output in the AVHRR data, followed by a steady increase in thermal output in the ASTER data, which lasts longer than 21 days. Whereas this transition is observable in the 2007 ASTER data due to the increased number of available scenes, the 2009 data presents a challenge for determining this transition to Phase III. From June 12 to July 4, 2009 there were no cloud-free ASTER scenes acquired. Solely based on the 2009 ASTER data (Fig. 3) one would conclude that the precursory activity transitions from Phase II to Phase III on 12 June 2009. However, by including the higher temporal resolution AVHRR data, there is a much improved opportunity for capturing a cloud-free scene. For example, a large thermal detection was observed in the AVHRR data on June 20, 2009. The event corresponds with a large strombolian eruption equivalent to the one that indicated the transition to Phase III in the 2007 precursory activity. ASTER data cannot confirm this transition point directly; however, it is clear based on the 2009 dataset, that if more clear ASTER data were available in 2007, the large conduit-clearing event on June 20, 2007 would mark the actual transition from Phase II to Phase III. With definitions of these transition points and intensity of thermal activity in each phase, it is possible to distinguish the precursory activity phase and time before the onset of a larger eruption.

Including ASTER data in the precursory activity timeline allows the period of fluctuations associated with the onset of an eruption to be increased from six days to four months. Within this four-month period two distinct phases were identified. Consistent fluctuations in thermal output occur with a minimal rise in the average of thermal output were detected approximately two to four months before the eruption. Approximately 2 months before to the onset of the 2009 eruption, the activity shifts to a consistent increase in thermal output. Similar activity was also observed before both the 2005 and 2007 eruptions; however the consistent increase is less obvious for reasons explained in this study. This distinction in activity occurs as the eruption cycle nears its onset can also be used to improve the accuracy in predicting the time of eruption.

4.2. Implementation into volcano monitoring

Many geophysical and remote sensing networks are currently used to monitor volcanic activity, including seismic, deformation, hydrology, gas as well as ground-based and orbital remote sensing datasets. The USGS assesses the capability of thermal remote sensing in volcanic monitoring, acknowledging its importance in monitoring increased heat flow that may result from magma ascent (Freymueller et al., 2008). It also mentions that tracking the thermal emission over time could play an important role in understanding volcanic unrest. However, when this report was written, thermal monitoring was confined to low spatial/high temporal resolution orbital data to classify particular types of volcanic activity after an eruption had begun. Including a higher spatial resolution sensor such as ASTER to the existing monitoring system provides a guideline for Phase II to Phase III activity. These guidelines are: (1) a change of more than 2 °C in thermal output at the summit in less than 1 week (Phase II transition); and (2) a sustained increase in thermal output lasting more than 21 days that is preceded by a large spike in thermal output in AVHRR or MODIS data (Phase III transition).

Currently, no quantitative values relating to the time before an eruption or the degree of activity are assigned to the color code levels used to communicate the eruptive state of a volcano. The limitation with these color coded systems is that the distinction between Green (normal conditions), Yellow (unrest), and Orange (heightened unrest with expectation of eruption) is a judgment call by the observatory scientists (Guffanti and Miller, 2013). However, including ASTER data into an already established monitoring system using AVHRR and MODIS data, precursory activity can be classified and quantitative values assigned to each color codes. For example, Phase I would be equivalent to green (normal) activity, Phase II to yellow (advisory), and Phase III to orange (watch). The criteria for the red (warning) level would not change as it signifies the eruption onset (Fig. 9). The inclusion of these data therefore should provide a quantitative transition to the next color code as well as provide insight into the potential hazards associated with each code as well as a good approximation of the eruption timing.

4.3. Phase III activity in 2007

The precursory activity for the 2007 VEI 2 eruption showed slight differences from the 2005 and 2009 eruptions. In both the 2005 and 2009 eruptions a period of VEI 1 eruptions preceded the VEI 2 eruption by approximately 4–6 months. The constant presence of precursory activity between these active periods indicates that the prior VEI 1 eruptions were linked to the later VEI 2 eruptions. Before the 2007 eruption there was no VEI 1 period. Also, during Phase III of the 2007 eruption there existed a period of lower thermal output lasting approximately two weeks. This preceded a large increase in thermal output followed by the eruption approximately 10 days later. Closer observation of the summit region in the ASTER data provides evidence of what may be occurring (Fig. 6). The majority of thermal output is being detected in four pixels centered on the primary vent within the crater (Fig. 6A). One week later (Fig. 6B/E), these four pixels are no longer thermally-elevated, likely due to the conduit being blocked by backfill. During this period the size of the thermal anomaly expanded by a 5% despite the average temperature drop. This increase in total area is likely the result of the expansion of the crater fumarole field, which would provide new pathways for gas now blocked at the primary vent. The total heat released during this period is lower than that recorded earlier, indicating pressure and heat is being blocked. As pressure builds below the blocked vent, a threshold is reached and a large strombolian/volcanian vent-clearing eruption occurs, likely expanding the diameter of the conduit and increasing the thermal output. The newly cleared vent is visible three weeks later (February 15, 2007). In Fig. 6C the 4 hottest pixels have temperatures once again higher than the surrounding pixels. However, in this case the area encompasses more than four pixels and reaches temperatures as high as 75 °C above background. The production of an expanded dominant vent also reduces in the size of the thermal anomaly to 0.67 km^2. This suggested that previous smaller (and more widely distributed) fumarole pathways are no longer active (or greatly reduced in activity as not to be detected by ASTER). A somewhat similar process was described in the Oppenheimer et al., (1993) analysis of Lascar volcano. It was believed that the explosive event that occurred in August 1986 at Lascar was triggered following the emplacement and solidification of a lava dome, which was proposed to impeded the degassing from fumaroles. An increase in pressure occurred as a result of the presence of the dome which then triggered an explosive eruption. At Kliuchevskoi, no dome was present that would have impeded the thermal output. However, it is possible the rollback of ejecta in the vent from the strombolian eruptions detected in the

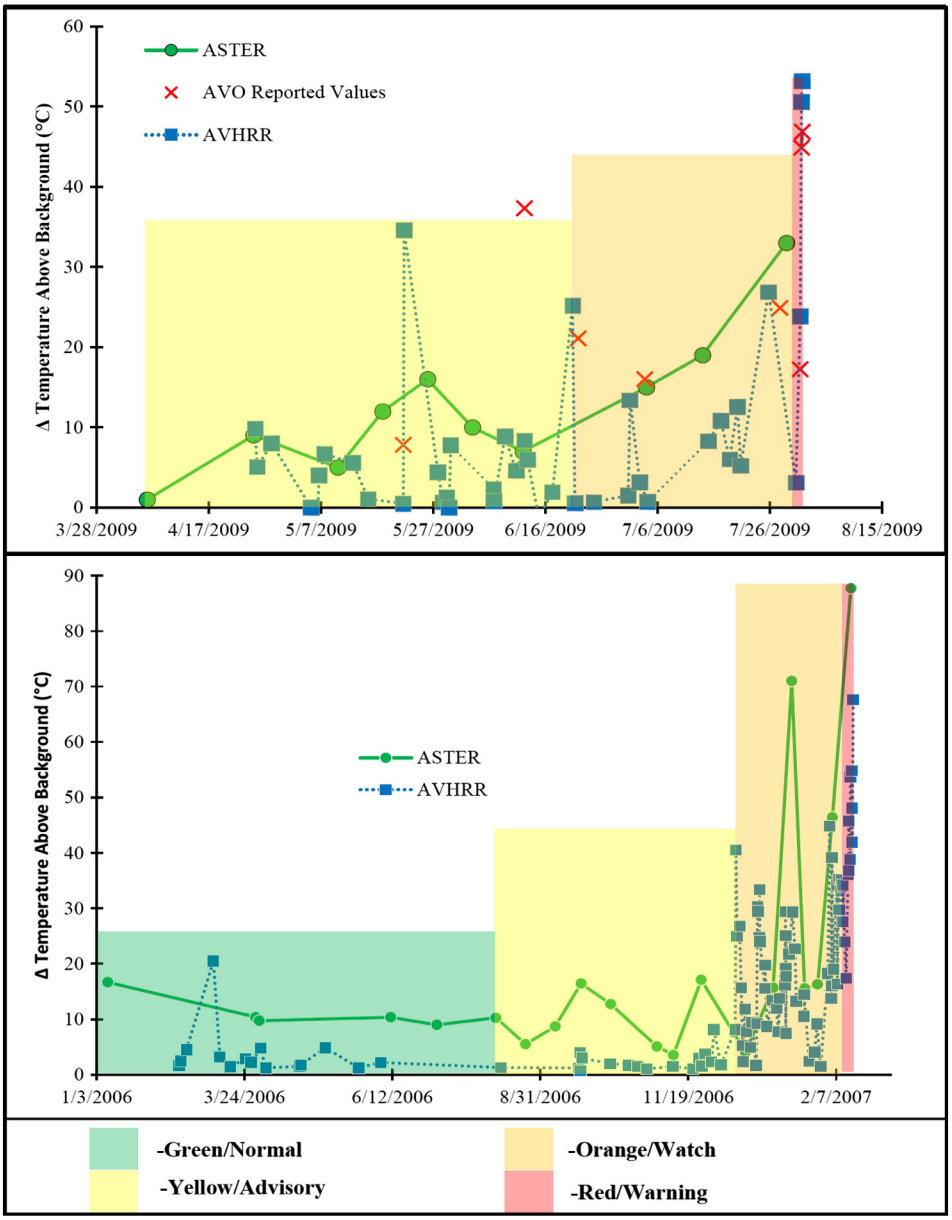

Fig. 9. Plot of 2009 and 2007 precursory activity shown together with the color code levels. The correlation between the thermal precursory phases and the color codes can be seen.

TIR data prior to the decrease in thermal output or the slumping of the inner conduit, destabilized from strombolian eruptions, walls may have blocked or partially blocked the dominant pathway. Once this blockage was cleared and the vent expanded, confining pressure on the magma chamber was greatly reduced, allowing for a rapid rise in magma height and the subsequent VEI 2 eruption.

4.4. Detection of strombolian eruptions

Many strombolian eruptions have been observed at Kliuchevskoi (Gushchenko, 1979; Rose and Ramsey, 2009; Smithsonian Global Volcanism Program, 2013). Research performed on Stromboli Volcano by Worden et al., (2014) demonstrates that in order to record a thermal increase from a strombolian eruption, a satellite overpass must occur within one minute of that eruption. This demonstrates that with the average number of strombolian eruptions that occur daily, a sensor with at least five overpasses per day to record this thermal signal. The temporal resolution of AVHRR (15 min to 6 h depending on the latitude and orbital configuration of the satellites carrying the AVHRR sensors) therefore suggests a strong likelihood that data are acquired soon after recently-deposited material at Kliuchevskoi. The spatial resolution of AVHRR constrains thermal detection to relatively large eruption events. Each spike in the AVHRR data therefore likely corresponds to a strombolian eruption of varying intensities (Dehn et al., 2000). This can now be confirmed with the addition of the ASTER data captured before and after one of these transient thermal events, which shows a large thermal anomaly at the summit quickly cooling over time. For example, on May 21, 2009 AVHRR data detected a larger than average thermal increase that was shown in ASTER data acquired five days later to have a size, shape and temperature profile expected for a moderately-size strombolian event. This same material was not evident 11 days before the AVHRR detection. Furthermore, a day after the ASTER image was acquired; AVHRR detected a thermal anomaly found to be 5.9 °C above background using the thermally integrated pixel Eq. (1). This material is cooling quickly, suggesting that it is thick enough to radiate heat to produce a thermal anomaly in AVHRR for close to a week.

4.5. Limitations

The combined use of both AVHRR and ASTER data does improve the fidelity of the TIR precursory interpretations, however there are limitations. For example, in some cases the lack of temporal resolution of the ASTER sensor reduces the ability to make more accurate interpretations (e.g., the precursory period before the 2005 eruption). This could be the case at other volcanoes that have persistent cloud cover or where the ASTER URP program has not acquired improved temporal datasets. Important information may still be gained from these sparse data through visual examination. This would be made more difficult however, if the data were examined without knowledge of the precursory patterns during a pre-established time period. Of concern are volcanoes in locations closer to the equator that are not observed under the URP program. This lack of data could be exacerbated by a combination of the poorer temporal frequency at the equator coupled with the common increased amount of clouds in tropical regions. Although it is still possible to collect enough clear ASTER scenes to make use of this precursory interpretation method, its likelihood is decreased in these situations.

4.6. Future precursory detection

A concern with the use of any ASTER data is the age of the sensor. It has exceeded its original six-year mission life by over ad decade at the time of this study. One ASTER subsystem, the shortwave infrared (SWIR), failed in 2008. There is, therefore, a great need for reliable, high-resolution, accurate TIR data from orbit. One possible solution is the planned Hyperspectral Infrared Imager (HyspIRI) sensor, which has not been officially approved by NASA and is subject to the outcome of the next NASA Earth Science decadal survey. The notional design of HyspIRI is to have a combined multispectral TIR sensor and a hyperspectral VSWIR sensor. The spatial resolution could be as small as 30 m and the TIR temporal resolution would improve to five days at the equator and one day closer to the poles (Roberts et al., 2012). This would be a substantial increase in both spatial and temporal resolutions, with both being critical to the approach presented here. A more complete high spatial resolution dataset, similar to the ASTER URP data now available for the northern Pacific volcanoes, would be possible in an increased amount of locations (Ramsey et al., 2013). The HyspIRI TIR dataset would reduce the temporal gaps and provide coverage of volcanoes in tropical regions, thus allowing this approach to be expanded to active volcanoes throughout the world. Furthermore, the improved spatial resolution would produce more accurate visual and thermal interpretations of smaller-scale activity, critical for precursory studies.

5. Conclusions

This study focused on three specific eruptions of Kliuchevskoi volcano and identified three distinct phases of precursory activity leading up to a larger eruption. In Phase I the thermal output produced at the crater remains relatively constant, similar to the heat produced during the typical, restive state of the volcano. In Phase II the thermal output becomes more variable, likely driven by the creation and rise of gas slugs causing magma levels in the conduit to rise. The transition from increasing to decreasing thermal output are marked by a series of strombolian eruptions that expel the gas, erupt hot material onto the flanks, and allow conduit magma levels to drop thereby reducing the thermal output. This cycle is detected up to six months prior to the larger eruption and typically ends approximately six weeks prior to that eruption. In Phase III the thermal output will consistently increase until the onset of the eruption. In this phase confining pressure in the magma pressure is reduced to the point where magma consistently rises in the conduit. Each of these phases can also be placed into the context of the current color codes for volcanic monitoring. Phase I corresponds to green (normal) conditions; Phase II to yellow (advisory) conditions; Phase III to orange (watch) conditions; and the actual eruption onset to red (warning) conditions. Coupling these phases with the warning codes in place provides a more quantitative reference frame to implement these codes, allowing them to be correlated with thermal output, the levels of activity, and the time before an eruption.

The approach presented here may not be universally applicable to all volcanoes depending on the data availability and style of precursory activity. However, similar thermal precursory studies are needed on a range of volcanoes, with different eruptive styles, locations, and data availability to confirm this statement. In doing, the warning period before future eruptions could be increased, giving local populations greater time to prepare, evacuate and reduce the risk to life and property.

The ability to accurately interpret volcanic precursory activity prior to an eruption improves the chances of accurately forecasting the later onset of a larger eruption. There are volcanoes that produce interpretable thermal precursory activity months to weeks prior to a larger eruption and by carefully monitoring and interpreting current satellite-based data, this activity can be tracked. Many volcanoes, however, produce seemingly random heat patterns before an eruption, which may not be clearly identified as precursory activity until very near the eruption onset. The precursory approach of this study tries to improve the interpretations of these seemingly random heat patterns by combining high temporal resolution data (e.g., AVHRR and MODIS) with high spatial resolution data (e.g., ASTER). The results show that the accuracy of forecasting a larger eruption and the lead time needed to do so is greatly improved. Data availability will continue to worsen, however, with the current fleet of aging and/or failing (e.g., Landsat 8 TIRS) high spatial resolution TIR sensors and no firm commitment for replacement.

Acknowledgements

Funding for this research was made possible by NASA under the Science of Terra and Aqua Research Program (NNX11AL29G and NNX14AQ96G) and the ASTER Science Team. The research presented here would not have been possible with the support of the people and programs available through AVO and V-ADAPT, Inc. The authors would like to thank the two anonymous reviewers whose time and detailed edits greatly improved the quality of this manuscript.

References

Abrams, M., 2000. The advanced spaceborne thermal emission and reflection radiometer (ASTER): data products for the high spatial resolution imager on NASA's Terra platform. Int. J. Remote Sens. 21 (5), 847–859.
Bailey, J.E., Dean, K.G., Dehn, J., Webley, P.W., 2010. US Geological Survey. Integrated Satellite Observations of the 2006 Eruption of Augustine Volcano (No. 1769–20).
Belousov, A., Belousova, M., Voight, B., 1999. Multiple edifice failures, debris avalanches and associated eruptions in the Holocene history of Shiveluch volcano, Kamchatka, Russia. Bull. Volcanol. 61 (5), 324–342.
Blackburn, E.A., Wilson, L., Sparks, R.S.J., 1976. Mechanisms and dynamics of strombolian activity. J. Geol. Soc. Lond. 132, 429–440.
Booth, B., Walker, G.P.L., 1973. Ash deposits from the new explosion crater, Etna 1971. Phil. Trans. R. Soc. London A274, 147–161.
Braitseva, O.A., Melekestsev, I.V., Ponomareva, V.V., Sulerzhitsky, L.D., 1995. Ages of calderas, large explosive craters and active volcanoes in the Kuril-Kamchatka region, Russia. Bull. Volcanol. 57 (6), 383–402.
Calvari, S., Pinkerton, H., 2004. Birth, growth and morphologic evolution of the "Laghetto" cinder cone during the 2001 Etna eruption. J. Volcanol. Geotherm. Res. 132, 225–239.
Carter, A.J., Girina, O., Ramsey, M.S., Demyanchuk, Y.V., 2008. ASTER and field observations of the 24 December 2006 eruption of Bezymianny volcano, Russia. Remote Sens. Environ. 112 (5), 2569–2577.
Carter, A.J., Ramsey, M.S., 2009. ASTER-and field-based observations at Bezymianny volcano: focus on the 11 may 2007 pyroclastic flow deposit. Remote Sens. Environ. 113 (10), 2142–2151.
Carter, A., Ramsey, M., 2010. Long-term volcanic activity at Shiveluch volcano: nine years of ASTER spaceborne thermal infrared observations. Remote Sens. 2 (11), 2571–2583.
Casadevall, T.J., 1993. US Geological Survey Open-File Report. Volcanic Ash and Airports: Discussion and Recommendations From the Workshop on Impacts of Volcanic Ash on Airport Facilities. 93, p. 518.
Chouet, B., Hamisevicz, N., McGetchin, T.R., 1974. Photoballistics of volcanic jet activity at Stromboli, Italy. J. Geophys. Res. 79, 4961–4976.

Chouet, B., Saccorotti, G., Dawson, P., Martini, M., Scarpa, R., De Luca, G., Milana, G., Cattaneo, M., 1999. Broadband measurements of the sources of explosions at stromboli volcano. Geophys. Res. Lett. 26, 1937–1940.

Dean, K., Dehn, J., McNutt, S., Neal, C., Moore, R., Schneider, D., 2002. Satellite imagery proves essential for monitoring erupting Aleutian volcano. Eos, Trans. AGU 83 (22), 241–247.

Dean, K., Servilla, M., Roach, A., Foster, B., Engle, K., 1998. Satellite monitoring of remote volcanoes improves study efforts in Alaska. Eos, Trans. AGU 79 (35), 413–423.

Dehn, J., Dean, K.G., Engle, K., 2000. Thermal monitoring of North Pacific volcanoes from space. Geology 28, 755–758.

Dehn, J., Dean, K.G., Engle, K., Izbekov, P., 2002. Thermal precursors in satellite images of the 1999 eruption of Shishaldin volcano. Bull. Volcanol. 64 (8), 525–534.

Dehn, J., and Harris, A. J. L., 2015. Thermal anomalies at volcanoes, Chapter 3 in Volcanoes of the North Pacific: Observations from Space. eds. Ken Dean and Jonathan Dehn. (In Press).

Duda, K.A., Ramsey, M., Wessels, R.L., Dehn, J., 2009. Optical Satellite Data Volcano Monitoring: A Multi-Sensor Rapid Response System. pp. 473–496.

Edwards, B., Belousov, A., Belousova, M., Volynets, A., Melnikov, D., Chirkov, S., Senyukov, S., Demianchuk, Y., 2013. Another "great Tolbachik" eruption? Eos, Trans. AGU 94 (21), 189–191.

Fearnley, C.J., McGuire, W.J., Davies, G., Twigg, J., 2012. Standardisation of the USGS Volcano Alert Level System (VALS): analysis and ramifications. Bull. Volcanol. 74 (9), 2023–2036.

Fedotov, S.A., 1984. The great Tolbachinsk fissure eruption-Kamchatka 1975-1976. Moscow Izdatel Nauka. 1.

Fedotov, S.A., Masurenkov, Y.P., 1991. Active volcanoes of Kamchatka, Vol. 1. Nauka, Moscow, p. 713.

Fedotov, S.A., Khrenov, A.P., Zharinov, N.A., 1987. Klyuchevskoy volcano, its activity in 1952–1986 and possible evolution. Volcanology and Seismology 6, 3–17 (in Russian). Miller, T. P., & Casadevall, T. J. (2000). Volcanic ash hazards to aviation. Encyclopedia of volcanoes, 915–930.

Francis, P., 1993. Volcanoes—A Planetary Perspective. Oxford University Press, Oxford.

Francis, P.W., Rothery, D.A., 1987. Using the Landsat thematic mapper to detect and monitor active volcanoes: an example from lascar volcano, northern Chile. Geology 15 (7), 614–617.

Freymueller, J.T., LaHusen, R.G., McGee, K.A., Poland, M.P., Power, J.A., Schmidt, D.A., ... White, R.A., 2008. Instrumentation Recommendations for Volcano Monitoring at US Volcanoes under the National Volcano Early Warning System (US Geological Survey).

Gillespie, A.R., 1985. Lithologic mapping of silicate rocks using TIMS. The TIMSData User's Workshop, June 18–19, 1985, JPL Pub. 86–38, pp. 29–44.

Gillespie, A., Rokugawa, S., Matsunaga, T., Cothern, J.S., Hook, S., Kahle, A.B., 1998. A temperature and emissivity separation algorithm for advanced spaceborne thermal emission and reflection radiometer (ASTER) images. IEEE Trans. Geosci. Remote Sens. 36 (4), 1113–1126.

Goita, K., Royer, A., 1997. Surface temperature and emissivity separability over land surface from combined TIR and SWIR AVHRR data. IEEE Trans. Geosci. Remote Sens. 35 (3), 718–733.

Gorshkov, G.S., 1959. Gigantic eruption of the volcano Bezymianny. Bull. Volcanol. 20 (1), 77–109.

Gushchenko, I.I., 1979. Eruptions of volcanoes of the world: a catalog. Academy of Science USSR Far Eastern Science Center. Nauka, Moscow, p. 474 (in Russian).

Guffanti, M., Miller, T.P., 2013. A volcanic activity alert-level system for aviation: review of its development and application in Alaska. Nat. Hazards 69 (3), 1519–1533.

Kirchdorfen, M., 1999. Analysis and quasistatic FE modeling of long period impulsive events associated with explosions at stromboli volcano (Italy). Ann. Geophys. 42, 379–391.

Koloskov, A.V., Gontovaya, L.I., Popruzhenko, S.V., 2014. The upper mantle of Kamchatka in isotopic-geochemical and geophysical anomalies: the role of asthenospheric diapirism. Russ. J. Pac. Geol. 8 (3), 151–162.

Kugaenko, Y., Saltykov, V., & Titkov, N. (2014, May). Pre-eruption deformation and seismic anomalies in 2012 in Tolbachik volcanic zone, Kamchatka. In EGU General Assembly Conference Abstracts (Vol. 16, p. 4548).

Harris, A.J., Butterworth, A.L., Carlton, R.W., Downey, I., Miller, P., Navarro, P., Rothery, D.A., 1997a. Low-cost volcano surveillance from space: case studies from Etna, Krafla, Cerro Negro, Fogo, Lascar and Erebus. Bull. Volcanol. 59 (1), 49–64.

Harris, A.J.L., Blake, S., Rothery, D.A., Stevens, N.F., 1997b. A chronology of the 1991 to 1993 Mount Etna eruption using advanced very high resolution radiometer data: implications for real-time thermal volcano monitoring. J. Geophys. Res. 102 (B4), 7985–8003.

Heiken, G., Casadevall, T.J., Newhall, C., 1992. First international symposium on volcanic ash and aviation safety. Bull. Volcanol. 54 (3), 250–251.

Harris, A.J.L., Wright, R., Flynn, L.P., 1999. Remote monitoring of Mount Erebus volcano, Antarctica, using polar orbiters: progress and prospects. Int. J. Rem. Sens. 20 (15–16), 3051–3071.

Jiang, G., Zhao, D., Zhang, G., 2009. Seismic tomography of the Pacific slab edge under Kamchatka. Tectonophysics 465 (1), 190–203.

Macdonald, G.A., 1972. Volcanoes. Prentice-Hall, Englewood Cliffs, NJ.

Marchese, F., Falconieri, A., Pergola, N., Tramutoli, V., 2014. A retrospective analysis of the Shinmoedake (Japan) eruption of 26–27 January 2011 by means of Japanese geostationary satellite data. J. Volcanol. Geotherm. Res. 269, 1–13.

Menyailov, I.A., 1975. Prediction of eruptions using changes in composition of volcanic gases. Bull. Volcanol. 39 (1), 112–125.

Miller, T.P., Casadevall, T.J., 2000. Volcanic ash hazards to aviation. Encyclopedia of Volcanoes, pp. 915–930.

Neal, C., Girina, O., Senyukov, S., Rybin, A., Osiensky, J., Izbekov, P., Ferguson, G., 2009. Russian eruption warning systems for aviation. Nat. Hazards 51 (2), 245–262.

Oppenheimer, C., Francis, P.W., Rothery, D.A., Carlton, R.W., Glaze, L.S., 1993. Infrared image analysis of volcanic thermal features: Lascar volcano, Chile, 1984–1992. J. Geophys. Res. Solid Earth 98 (B3), 4269–4286 (1978–2012).

Ozerov, A., Ariskin, A., Kyle, P., Bogoyavlenskaya, G., Karpenko, S., 1997. Petrological-geochemical model for genetic relationships between basaltic and andesitic magmatism of Klyuchevskoi and Bezymiannyi volcanoes, Kamchatka. Petrology 5 (6), 550–569.

Patrick, M.R., Harris, A.J., Ripepe, M., Dehn, J., Rothery, D.A., Calvari, S., 2007. Strombolian explosive styles and source conditions: insights from thermal (FLIR) video. Bull. Volcanol. 69 (7), 769–784.

Parfitt, E.A., 2004. A discussion of the mechanisms of explosive basaltic eruptions. J. Volcanol. Geotherm. Res. 134, 77–107.

Parfitt, E.A., Wilson, L., 1995. Explosive volcanic eruptions—IX. The transition between Hawaiian-style lava fountaining and Strombolian explosive activity. Geophys. J. Int. 121, 226–232.

Pergola, N., D'Angelo, G., Lisi, M., Marchese, F., Mazzeo, G., Tramutoli, V., 2009. Time domain analysis of robust satellite techniques (RST) for near real-time monitoring of active volcanoes and thermal precursor identification. Phys. Chem. Earth, Parts A/B/C 34 (6), 380–385.

Pergola, N., Marchese, F., Tramutoli, V., 2004. Automated detection of thermal features of active volcanoes by means of infrared AVHRR records. Remote Sens. Environ. 93 (3), 311–327.

Pieri, D., Abrams, M., 2005. ASTER observations of thermal anomalies preceding the April 2003 eruption of Chikurachki volcano, Kurile Islands, Russia. Remote Sens. Environ. 99 (1), 84–94.

Portnyagin, M., Hoernle, K., Avdeiko, G., Hauff, F., Werner, R., Bindeman, I., ... Garbe-Schönberg, D., 2005. Transition from arc to oceanic magmatism at the Kamchatka-Aleutian junction. Geology 33 (1), 25–28.

Ramsey, M., Dehn, J., 2004. Spaceborne observations of the 2000 Bezymianny, Kamchatka eruption: the integration of high-resolution ASTER data into near real-time monitoring using AVHRR. J. Volcanol. Geotherm. Res. 135 (1), 127–146.

Ramsey, M., Dehn, J., Wessels, R., Byrnes, J., Duda, K., Maldonado, L., Dwyer, J., 2004. The ASTER emergency scheduling system: a new project linking near-real-time satellite monitoring of disasters to the acquisition of high-resolution remote sensing data. AGU Fall Meeting Abstracts. 1, p. 0026.

Ramsey, M.S., Reath, K.A., Williams, D.B., 2013. Threshold Considerations for Future Volcanic Hotspot and Ash Detection Using HysplRI, 2013 HysplRI Science Workshop, Pasadena, CA.

Ramsey, M.S., 2015. Synergistic use of satellite thermal detection and science: a decadal perspective using ASTER, detecting, modelling and responding to effusive eruptions. In: Harris, A., De Groeve, T., Garel, F., Carn, S.A. (Eds.), Detecting, Modelling and Responding to Effusive Eruptions, Geol. Soc., London, Special Publications, p. 426 (in press).

Realmuto, V.J., 1990. Separating the effects of temperature and emissivity: emissivity spectrum normalization. Proceedings of the 2nd TIMS Workshop. 2, pp. 31–35.

Reath, K.A., Ramsey, M.S., 2013. Exploration of geothermal systems using hyperspectral thermal infrared remote sensing. J. Volcanol. Geotherm. Res. 265, 27–38.

Ripepe, M., Marchetti, E., 2002. Array tracking of infrasonic sources at Stromboli Volcano. Geophys. Res. Lett. 29, 2076.

Ripepe, M., Rossi, M., Saccorotti, G., 1993. Image processing of explosive activity at Stromboli. J. Volcanol. Geotherm. Res. 54, 335–351.

Roberts, D.A., Quattrochi, D.A., Hulley, G.C., Hook, S.J., Green, R.O., 2012. Synergies between VSWIR and TIR data for the urban environment: an evaluation of the potential for the hyperspectral infrared imager (HysplRI) decadal survey mission. Remote Sens. Environ. 117, 83–101.

Rose, S., Ramsey, M., 2009. The 2005 eruption of Kliuchevskoi volcano: chronology and processes derived from ASTER spaceborne and field-based data. J. Volcanol. Geotherm. Res. 184 (3), 367–380.

Rothery, D.A., Francis, P.W., Wood, C.A., 1988. Volcano monitoring using short wavelength infrared data from satellites. J. Geophys. Res. Solid Earth 93 (B7), 7993–8008. (1978–2012).

Schneider, D.J., Dean, K., Dehn, J., Miller, T., Kirianov, V.Y., 2000. Monitoring and analyses of volcanic activity using remote sensing data at the Alaska volcano observatory: case study for Kamchatka, Russia, December 1997. Remote Sensing of Active Volcanism, pp. 65–85.

Self, S., Sparks, R.S.J., Booth, B., Walker, G.P.L., 1974. The 1973 Heimaey strombolian scoria deposit, Iceland. Geol. Mag. 111 (06), 539–548.

Smithsonian Institute, 2013. Kliuchevskoi Volcano Eruptive History, Global Volcanism Program. 12/5/2013 http://www.volcano.si.edu/volcano.cfm?vn=300260.

Sobolevskaya, O.V., Senyukov, S.L., 2008. Retrospective analysis of the thermal anomaly temperature change at bezymianny volcano 2002-2007, as a precursor of it's eruptions, by avhrr noaa 16 and 17 satellite data. Bulletin of Kamchatka regional association 'educational-scientific center'. Earth Sci. 11, 147–157.

Thome, K., Arai, K., Hook, S., Kieffer, H., Lang, H., Matsunaga, T., ... Takashima, T., 1998. ASTER preflight and inflight calibration and the validation of level 2 products. IEEE Trans. Geosci. Remote Sens. 36 (4), 1161–1172.

van Manen, S.M., Dehn, J., 2009. Satellite remote sensing of thermal activity at Bezymianny and Kliuchevskoi from 1993 to 1998. Geology 37 (11), 983–986.

van Manen, S.M., Dehn, J., Blake, S., 2010. Satellite thermal observations of the Bezymianny lava dome 1993–2008: precursory activity, large explosions, and dome growth. J. Geophys. Res. Solid Earth 115 (B8) (1978–2012).

van Manen, S.M., Blake, S., Dehn, J., Valcic, L., 2013. Forecasting large explosions at Bezymianny volcano using thermal satellite data. Geol. Soc. Lond., Spec. Publ. 380 (1), 187–201.

Webley, P.W., Lopez, T.M., Ekstrand, A.L., Dean, K.G., Rinkleff, P., Dehn, J., ... Worden, A., 2013. Remote observations of eruptive clouds and surface thermal activity during the 2009 eruption of redoubt volcano. J. Volcanol. Geotherm. Res. 259, 185–200.

Worden, A., Dehn, J., Webley, P., 2014. Frequency based satellite monitoring of small scale explosive activity at remote North Pacific volcanoes. J. Volcanol. Geotherm. Res. 286, 1–14.
Wright, R., Flynn, L.P., Garbeil, H., Harris, A.J., Pilger, E., 2004. MODVOLC: near-real-time thermal monitoring of global volcanism. J. Volcanol. Geotherm. Res. 135 (1), 29–49.
Vergniolle, S., Brandeis, G., 1996. Strombolian explosions. 1. A large bubble breaking at the surface of a lava column as a source of sound. J. Geophys. Res. 101, 20433–20447.
Yamaguchi, Y., Kahle, A.B., Tsu, H., Kawakami, T., Pniel, M., 1998. Overview of advanced spaceborne thermal emission and reflection radiometer (ASTER). IEEE Trans. Geosci. Remote Sens. 36 (4), 1062–1071.
Yogodzinski, G.M., Lees, J.M., Churikova, T.G., Dorendorf, F., Wöerner, G., Volynets, O.N., 2001. Geochemical evidence for the melting of subducting oceanic lithosphere at plate edges. Nature 409 (6819), 500–504.